

Cite this article as: Zhou Anyang, Huang Yanfei, Guo Weiling, et al. Effect of Pulsed Magnetic Field Strength on Mechanical and Micro-motion Wear Properties of GH99 Nickel-Based Alloy[J]. Rare Metal Materials and Engineering, 2024, 53(02): 330-344. DOI: 10.12442/j.issn.1002-185X.20230341.

ARTICLE

Effect of Pulsed Magnetic Field Strength on Mechanical and Micro-motion Wear Properties of GH99 Nickel-Based Alloy

Zhou Anyang¹, Huang Yanfei¹, Guo Weiling¹, Xing Zhiguo¹, Wang Haidou^{1,3}, Wang Zhiyuan⁴, Zhang Yanfang²

¹National Key Laboratory for Remanufacturing, Army Academy of Armored Forces, Beijing 100072, China; ²Department of Stomatology, The Seventh Medical Center, Chinese PLA General Hospital, Beijing 100000, China; ³National Engineering Research Center for Remanufacturing, Army Academy of Armored Forces, Beijing 100072, China; ⁴School of Materials Science and Engineering, Harbin Institute of Technology, Harbin 150001, China

Abstract: In order to investigate the influence of different magnetic field strengths on the mechanical property and wear resistance of nickel-based alloy, GH99 nickel-based alloy specimen was subjected to pulsed magnetic treatment by the pulsed strong magnetic field equipment. Through the microstructure observation, the wear mechanism and strengthening mechanism of GH99 nickel-based alloy were analyzed. Results show that the applied pulsed magnetic field improves the material dislocation distribution and reduces the dispersion of residual stress on the specimen surface. At the magnetic field strength of 10 T, the residual compressive stress reaches the maximum value (−223.45 MPa). The tensile fracture of the material is mainly characterized by the ductile fracture. This is because the pulsed magnetic field treatment of the alloy produces sub-structured dislocation cells, which contributes to the fine grain strengthening effect. In addition, the surface microhardness and wear resistance of the specimen are firstly increased and then decreased with increasing the magnetic field strength from 0 T to 15 T. The dislocations inside the alloy proliferate under the pulsed magnetic field, increasing the dislocation density and resulting in the phenomenon similar to the process hardening. However, excessive magnetic field strength may lead to the dislocation plugging, resulting in severe distortion of the cell dot and deterioration of material properties.

Key words: pulsed magnetic field; magnetic field strength; GH99 nickel-based alloy; mechanical property; wear resistance

GH99 nickel-based alloys are commonly used in the manufacture of high-temperature load-bearing components due to their high heat resistance, high-temperature oxidation resistance, and good corrosion resistance, thereby widely applied in the engine combustion chambers, turbine disks, blades, and other key components. However, due to the high contact stress and micron-scale tangential displacement^[1], damage or even failure easily occurs during the service. Therefore, the enhancement in wear resistance of GH99 nickel-based alloy under micro-motion condition gradually becomes a research hotspot.

The main strengthening methods of GH99 nickel-based

alloys include the heat treatment^[2] and solid solution strengthening^[3]. However, the high cost, introduction of heterogeneous crystals, and high energy consumption restrict the practical application. With the development of high-field magnetic field technique, magnetic field, as a strengthening tool, has been extensively used in the engineering field, because it can enhance the alloy performance without substrate contact and surface integrity damage. Pulsed magnetic fields can generate induced currents inside the solid alloys, and the electromagnetic force generated by the interactions between the current and the magnetic field can produce magnetic pressure, which can influence the alloy

Received date: June 01, 2023

Foundation item: National Natural Science Foundation of China (52275227, 52130509)

Corresponding author: Xing Zhiguo, Ph. D., Assistant Researcher, National Key Laboratory for Remanufacturing, Army Academy of Armored Forces, Beijing 100072, P. R. China, E-mail: xingzg2011@163.com

Copyright © 2024, Northwest Institute for Nonferrous Metal Research. Published by Science Press. All rights reserved.

properties to some extent. It is reported that the pulsed magnetic field treatment of high-speed steel can transform some residual austenite into hard and brittle martensite, achieving significant hardening effects^[4]. Wang et al^[5] found that the pulsed magnetic field treatment can rotate the magnetic domains of 20Cr2Ni4A steel. Magnetostriction induced by pulsed magnetic field treatment can increase the residual compressive stress near the surface, thus prolonging the contact fatigue life of 20Cr2Ni4A steel. Zhang et al^[6] found that the proportion of α -Fe phase in 20Cr2Ni4A steel increases by 10% under the pulsed magnetic field of 9 T, consequently improving the steel hardness. Ferromagnetic alloys are usually investigated under the pulsed magnetic field, whereas the non-magnetic alloys are rarely studied. In addition, the magnetic field strength for nonmagnetic alloys is generally as low as below 5 T^[7]. The relationship between the magnetic field strength and the strengthening effect of non-magnetic alloy properties is rarely discussed. Therefore, the microstructure change of GH99 nickel-based alloy under high-strength pulsed magnetic field and the resultant property change require further investigation.

In this research, the effect of pulsed magnetic field treatment on the property of non-magnetic GH99 nickel-based

alloy was investigated. By applying pulsed magnetic fields of different intensities, the residual stress, hardness, plasticity, and wear resistance of GH99 nickel-based alloy were analyzed. Besides, the mechanism of property change was discussed from the perspective of dislocation structure and grain structure.

1 Experiment

The non-magnetic GH99 nickel-based alloy was used as the experiment material, whose composition is listed in Table 1. The specimen was obtained by vacuum induction, electroslag remelting, and solid solution at 1120 °C. The specimen dimension for tensile tests is shown in Fig. 1. The GH99 nickel-based alloy specimens of 25 mm×10 mm×5 mm were prepared by wire-cutting. Among them, the plane with 25 mm×10 mm was selected as the testing surface, which was polished to mirror surface, ultrasonically cleaned in anhydrous ethanol for 15 min, and finally dried.

The high-frequency pulsed strong magnetic field equipment is mainly composed of a charger, capacitor, transistor switch, high voltage relay, energy drain switch, pulsed magnetic field magnet, fixture, synchronization control software, and oscilloscope. The magnetic field generated by the magnet had

Table 1 Main chemical components of GH99 alloy (wt%)

C	Si	Mn	S	P	Cr	Fe	W	Mo	Al	Ti	Co	B	Ce	Ni
0.046	0.16	0.02	0.001	0.006	18.02	1.60	6.0	3.92	2.24	1.21	6.04	<0.005	<0.02	Bal.

the pulse width of 8 ms, rising edge of 1 ms, and falling edge of 7 ms. In this research, the magnetic field strength was 5, 10, and 15 T in the center hole area of the magnet when the charging voltage was 1.58, 3.17, and 4.75 kV, respectively. The waveform generated by pulsed magnetic field is shown in Fig.2. The specimen was fixed on a resin cover with special fixture to prevent the flying-out phenomenon of specimen due to the electromagnetic force induced by strong pulsed magnetic field, as shown in Fig.3.

The fracture morphology of tensile specimens after treatment at different magnetic field strengths and the abrasion morphology of different specimens were observed by FEI Quanta 450 FEG scanning electron microscope (SEM). The chemical composition of abrasion surface was analyzed by energy dispersive spectrometer (EDS). X-ray diffractometer (XRD) and FEI Tecnai G2 F30 field emission transmission electron microscope (TEM) were also used to analyze the

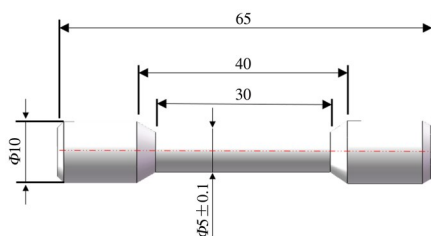


Fig.1 Schematic diagram of tensile specimen

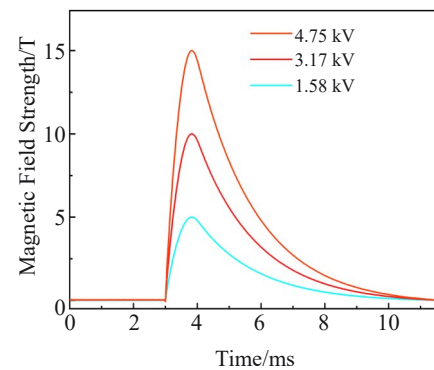


Fig.2 Waveform generated by different pulsed magnetic fields

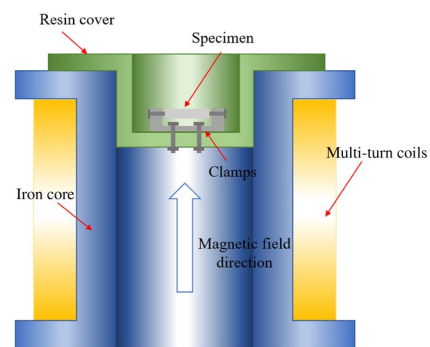


Fig.3 Schematic diagram of specimen fixture setup

dislocation structure of GH99 nickel-based alloy, as well as the dislocation density, dislocation morphology, and dislocation distribution observation.

The specimen hardness was measured by THV-1MD digital display automatic turret microhardness tester, and 20 points were selected for hardness measurement. The average hardness was used for analysis. The experiment conditions were loading force of 500 g and loading time of 10 s. Tensile tests were conducted by INSTRON-5582 material universal testing machine (UK). Tensile strength, elongation, and section shrinkage were obtained to evaluate the plasticity change of specimens. The experiments were conducted with elongation gauge of 15 mm and loading rate of $2 \text{ mm}\cdot\text{min}^{-1}$. The residual stress was measured by X-ray residual stress analyzer (PROTO IXRD). The measurement target was manganese, and the scanning angle range was between -20° and 20° . The test method was the isotropic fixed Ψ_0 method.

The micro-motion friction wear tests were conducted by the self-developed tangential micro-motion wear experiment equipment, as shown in Fig. 4. The test machine is mainly composed of control system, loading system, and driving system. The test parameters were normal load $F_n=30 \text{ N}$, displacement amplitude $D=\pm 40 \mu\text{m}$, and frequency $f=5 \text{ Hz}$. The workflow of this equipment was as follows: the lower specimen, i. e., block GH99 nickel-based alloy, was placed on the lower specimen fixture and tested at room temperature; the normal load was applied onto the lower specimen by stacking weights of different load sizes; the force sensor was equipped on

monitor and the applied load information was recorded in real time.

In the frictional wear process, Si_3N_4 ceramic balls with diameter of 8 mm were selected as the counterbalance material, and the ceramic balls were fixed by counterbalance fixture, forming the flat-ball contact. The mechanical properties of Si_3N_4 ceramic balls are listed in Table 2.

2 Results

2.1 Effect of pulsed magnetic treatment on residual stress of GH99 alloy

Fig. 5 shows the residual stress distributions on specimen surfaces without and with pulsed magnetic treatment at 5, 10, and 15 T. It can be seen that the residual stresses of all four

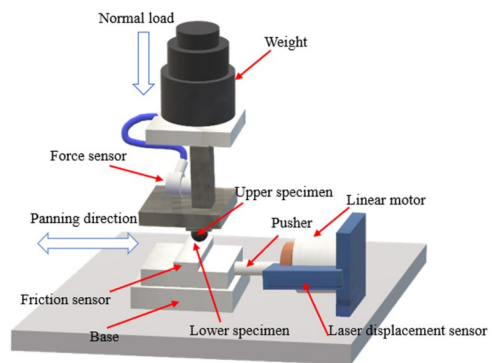


Fig.4 Schematic diagram of tangential micro-abrasion tester

Table 2 Mechanical properties of Si_3N_4 ceramic balls

Property	Hardness, HV/MPa	Density/ $\text{g}\cdot\text{cm}^{-3}$	Poisson's ratio	Surface roughness, $R_a/\mu\text{m}$	Fracture toughness/ $\text{MPa}\cdot\text{m}^{1/2}$
Value	13896.4	3.2	0.26	0.02–0.08	5–7

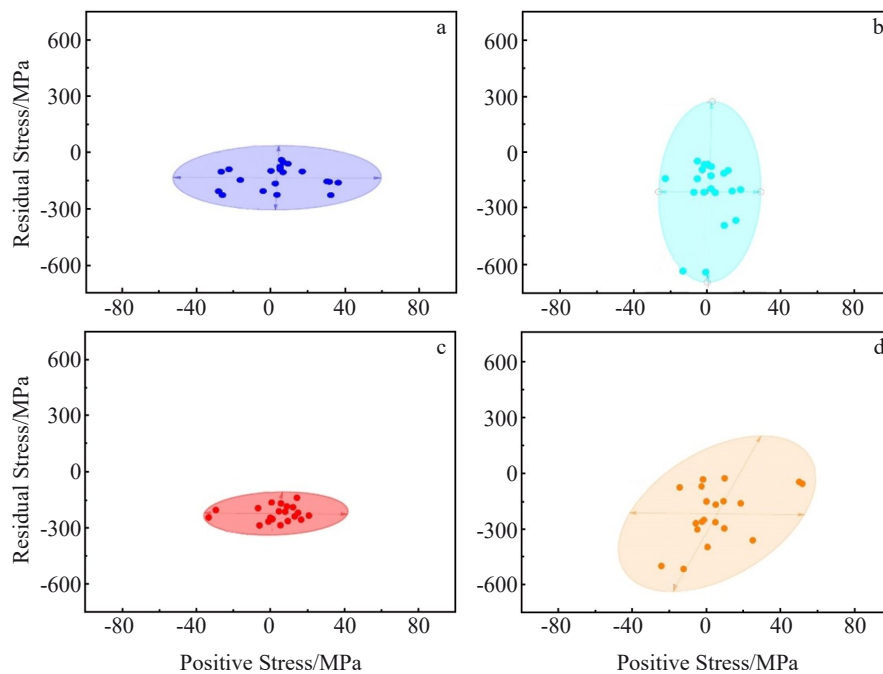


Fig.5 Residual stress distributions on GH99 alloy surface without (a) and with pulsed magnetic treatment at 5 T (b), 10 T (c), and 15 T (d)

specimens are compressive stresses, and there is a tendency of spontaneous compression phenomenon occurring on surface. According to Fig. 5a, without pulsed magnetic treatment, the overall distribution of residual stress is wide. Particularly, the residual stresses distributed along tangential direction are more dispersed. This result is closely related to the preparation process of GH99 nickel-based alloy. Fig. 6 shows the dislocation distributions of GH99 nickel-based alloy without pulsed magnetic treatment. It can be observed from Fig. 6a and 6b that the dislocations inside the specimens without pulsed magnetic treatment have different degrees of dislocation entanglement at grain boundaries and inside grains. The dislocation grouping is dominated by the accumulation of large dislocation clusters, which are surrounded by the dispersed small dislocation clusters. The dislocation clusters in Fig. 6 are consistent with the residual stress distributions in the specimens without pulsed magnetic treatment, because the dislocation accumulation usually leads to the residual stress concentration^[8].

Fig. 5b – 5d show the residual stress distributions on specimen surfaces with pulsed magnetic treatment at 5, 10, and 15 T, respectively. It can be seen that on the specimen surface with pulsed magnetic treatment at 5 T, the compressive stresses increase and the tangential stresses decrease, compared with those without pulsed magnetic treatment. With increasing the magnetic field strength to 10 T, the residual stress becomes more concentrated and homogenized, compared with those without pulsed magnetic treatment. This result shows that the pulsed magnetic treatment can improve the residual stress on the surface of GH99 nickel-based alloy. However, it is also found that the distribution of the residual stresses on the specimen surface with pulsed magnetic treatment at 15 T becomes highly dispersed. These results indicate that the pulsed magnetic field can ameliorate the residual stresses at low magnetic field strengths (5 and 10 T). The significant improvement under the condition of magnetic field strength at 10 T is attributed to the electromagnetic properties of internal dislocations^[9]. As a result, the activation energy of dislocation opening declines, resulting in easy dislocation slip inside the material, and the dislocation motion becomes more obvious. However, during the pulsed magnetic treatment with large field strength, such as 15 T, severe point

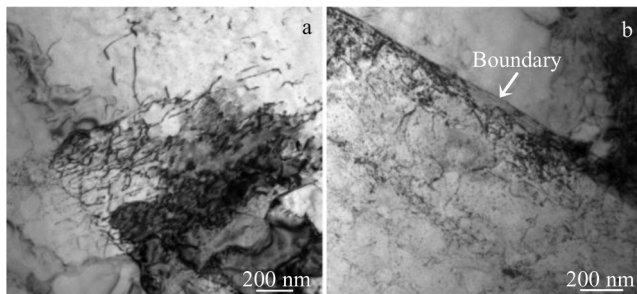


Fig.6 Dislocation distributions on GH99 alloy surface without pulsed magnetic treatment: (a) within grains and (b) at grain boundaries

distortions occur in the crystalline cells because of excessive dislocations at the grain boundaries and fine sub-crystalline tissues in crystals, therefore degrading the material properties. Thus, the magnetic field strength of 10 T is optimal.

Usually, the mean magnitude of residual stress expresses the residual stress at macro-level, and the standard deviation of residual stress reflects the residual stress at micro-level^[10]. Fig. 7 shows the average residual compressive stress of specimens without and with pulsed magnetic treatment at 5, 10, and 15 T, which is -135.88 , -212.85 , -223.45 , and -218.63 MPa, respectively. The surface compressive stress increases rapidly after applying the pulsed magnetic field. With increasing the magnetic field strength, the residual compressive stress barely changes. Averagely, the residual compressive stress of the specimens with pulsed magnetic treatment increases by 60.66%, compared with that without pulsed magnetic treatment, indicating that the pulsed magnetic treatment significantly increases the residual compressive stress of GH99 alloy. The smallest standard deviation is achieved for the specimen with pulsed magnetic treatment at 10 T, whereas the largest standard deviation is achieved for the specimen with pulsed magnetic treatment at 5 T. The internal grains or subgrains of GH99 alloy are affected by the pulsed magnetic treatment, resulting in the refinement of internal grains and thus changing the standard deviation values.

2.2 Effect of pulsed magnetic treatment on plasticity and strength of GH99 alloy

Fig. 8 shows the room-temperature tensile fracture morphologies of GH99 alloy specimens without and with pulsed magnetic treatment at different field strengths. The overall fracture morphologies are shown in the insets of Fig. 8a – 8d. It can be seen that the room-temperature tensile fracture of the specimen without pulsed magnetic treatment is relatively flat, showing river-like pattern and some steps. According to Fig. 8e, there are mainly destructive steps with a few tough nests, inferring that the specimen mainly suffers the brittle fracture. Besides, both the number and size of the tough nests are small (average diameter of about $4 \mu\text{m}$), and the nest depth is small, as indicated by the red arrows in Fig. 8e. These

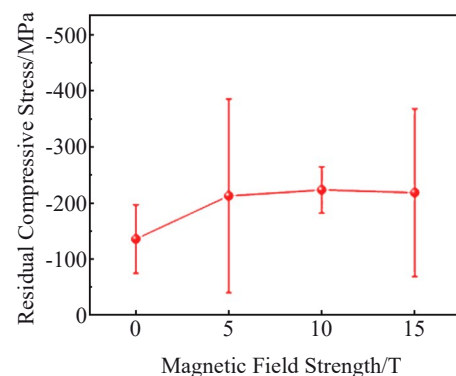


Fig.7 Residual compressive stresses on GH99 alloy surfaces without and with pulsed magnetic treatment at different field strengths

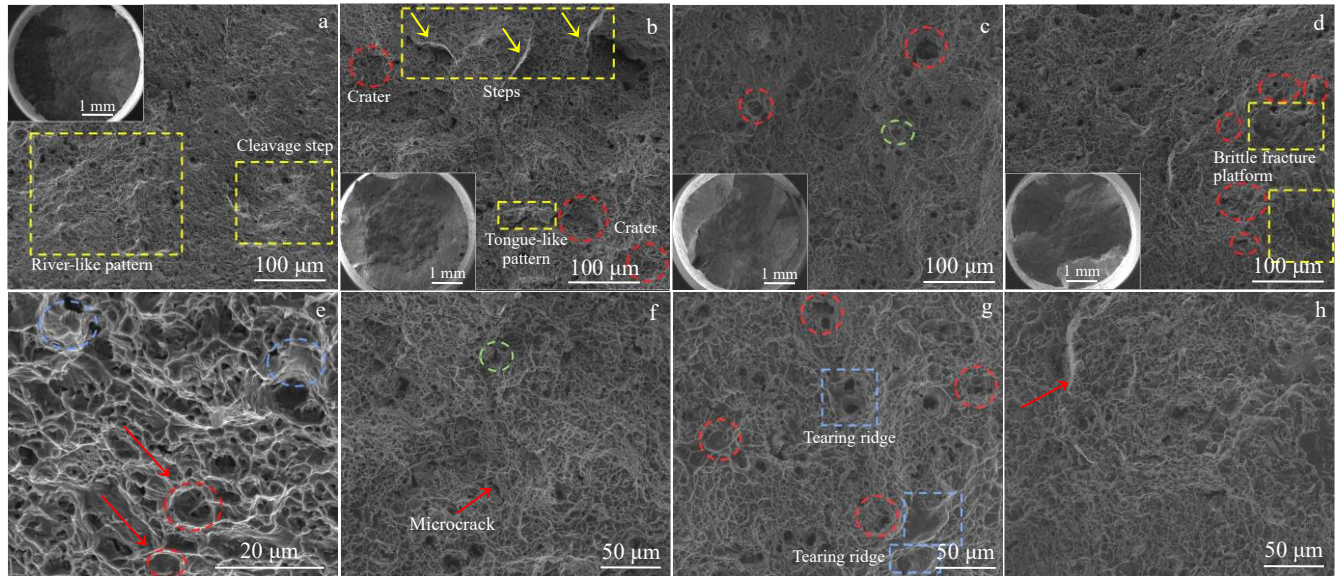


Fig.8 Room-temperature tensile fracture morphologies of GH99 alloy specimens without (a, e) and with pulsed magnetic treatment at 5 T (b, f), 10 T (c, g), and 15 T (d, h)

characteristics of tough nests suggest that the specimen plasticity is relatively inferior and the elongation is only 43.08%. Typical quasi-dissociation characteristics of fracture can be observed in the blue circles in Fig.8e^[11], implying that the quasi-dissociation is the dominant fracture mode for the specimen without pulsed magnetic treatment after room-temperature stretching.

As shown in Fig. 8b, the fracture morphology of the specimen with pulsed magnetic treatment at 5 T shows a mixed fracture mode, consisting of step-like deconvolution fracture and toughness fracture with tough nests. Craters can be observed in the red circles in Fig. 8b, which are relatively shallow and exhibit the deconvolution fracture characteristics. Additionally, a certain number of small ductile fractures and deconstruction steps (indicated by the yellow arrows) can also be observed, accompanied by a tongue-like pattern. This result indicates the deconstruction fracture with some plastic deformation. In Fig. 8f, some microcracks appear at the grain boundaries, as indicated by the red arrow; the reinforced phase particles can be found in the tough nests, as indicated by the green circle. EDS point scanning analysis was also conducted, and the results are shown in Fig. 9 and Table 3. The interactions between the reinforced phase particles and dislocations homogenize the size of tough nests and indirectly strengthen the specimen plasticity.

As shown in Fig. 8, the size of some tough nests (red circles) increases, the overall number of some tough nests increases significantly, the fracture becomes more severe, and the depth of tough nests increases, compared with those without pulsed magnetic treatment. As shown in Fig. 8g, tearing ridges become thicker and larger, and the petal-like shape appears (blue rectangle). These phenomena usually occur when the fracture mechanism is similar to the ductile fracture. According to Fig. 8c, some tough nests even have

small nests inside (red circles), indicating the enhancement in deformation resistance of the tensile specimens after pulsed magnetic treatment at 10 T. As shown in the inset of Fig.8c, the proportion of tough nests in the overall fracture area is the largest, compared with those without and with pulsed magnetic treatment at 5 and 15 T, indicating the optimal plastic deformation capacity. This phenomenon is also consistent with the results of the elongation and section shrinkage of the alloys in Fig.10.

As shown in the inset of Fig.8d, it is found that the fracture morphology of specimen with pulsed magnetic treatment at 15 T becomes more uneven and has deeper pits, compared with those without and with pulsed magnetic treatment at 5 T. According to Fig.8h, the number of tough nests also increases. Meanwhile, a small area occupied by brittle fracture platform can also be observed, as shown in the yellow rectangles. This phenomenon fits well with the elongation and section shrinkage results of the alloys with pulsed magnetic treatment at 10 T, as shown in Fig.10. The number of tough nests (red

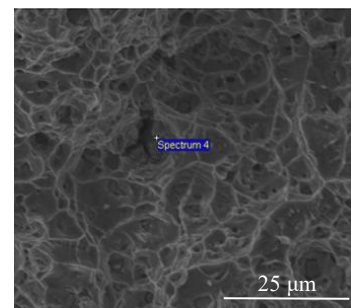


Fig.9 SEM morphology of reinforced phase particles inside tough nest of GH99 alloy specimen with pulsed magnetic treatment at 5 T

Table 3 EDS point scanning results of the point in Fig.9

Element	wt%	at%
C	8.32	30.79
Al	1.83	3.02
Ti	1.37	1.27
Cr	18.36	15.70
Fe	1.51	1.21
Co	4.99	3.76
Ni	54.34	41.15
Mo	3.82	1.77
W	5.46	1.32

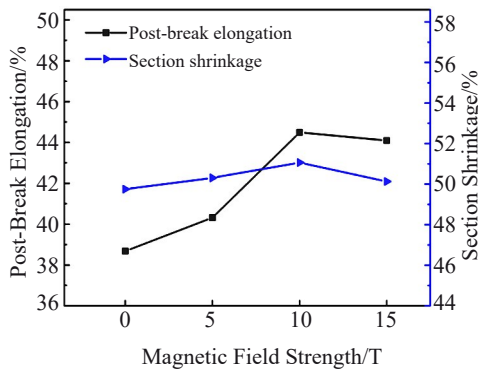


Fig.10 Effect of magnetic field strength on post-break elongation and section shrinkage of GH99 alloys

circles) with smaller sizes, which are uniformly distributed around the brittle fracture platform, increases obviously. The tough nests in Fig. 8d are mainly dominated by the round holes, presenting the obvious tendency of ductile fracture and indicating the improved plasticity of the alloy at this magnetic field conditions^[12]. As shown in Fig.8h, the tearing ridges (red arrow) of the fracture are thicker, compared with those without and with the pulsed magnetic treatment at 5 T.

Fig. 10 shows the effect of magnetic field strength on the post-break elongation and section shrinkage of GH99 alloys without and with pulsed magnetic treatment at different field strengths. It can be seen that the post-break elongation of specimens with pulsed magnetic treatment at 5, 10, and 15 T is 40.318%, 44.492%, and 44.094%, which is 1.638%, 5.812%, and 5.414% higher than that of the specimen without pulsed magnetic treatment, respectively. The post-break elongation increases rapidly when the magnetic field strength varies from 5 T to 10 T, and it decreases slightly when the magnetic field strength is 15 T. The section shrinkage also increases slightly with the increment of 2% or less after pulsed magnetic treatment at 5 and 10 T, whereas the section shrinkage decreases when the magnetic field strength further increases to 15 T. The grain refinement after the pulsed magnetic treatment plays an important role in the maintenance of good plasticity of specimens, which allows the grains to better coordinate with each other in deformation process.

The strong plastic product can characterize the overall

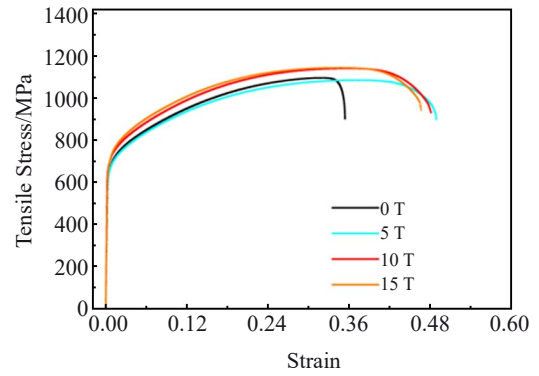


Fig.11 Tensile stress-strain curves of GH99 alloys without and with pulsed magnetic treatment at different field strengths

performance (strength and toughness) of alloys, and its value is approximately equal to the area enclosed by tensile curve. As shown in Fig. 11, the comprehensive mechanical properties (strong plastic product) of the specimens with pulsed magnetic treatment are higher than those without pulsed magnetic treatment, indicating that the pulsed magnetic treatment improves the plasticity and strength of GH99 nickel-based alloy to some extent, and the strengthening effect is enhanced. In addition, the tensile stress-strain curves show that GH99 nickel-based alloy does not present obvious yielding phenomenon, so the stress value $R_{p0.2}$, which is measured when the residual strain is 0.2%, is used as the yield strength of specimens in this research. The yield strength and tensile strength of GH99 alloys without and with pulsed magnetic treatment at different field strengths are shown in Fig. 12. The yield strength of the specimen with pulsed magnetic treatment at 10 T reaches 713 MPa, which is higher than that without pulsed magnetic treatment by 41.2 MPa. The yield strength of the specimens with pulsed magnetic treatment at 5 and 15 T increases to a small extent by 15.8 and 25.4 MPa, respectively, compared with that without pulsed magnetic treatment. According to the Hall-Patch relationship, the grain size is closely related to the yield strength, as expressed by Eq.(1)^[13], as follows:

$$\sigma_y = \sigma_0 + kd^{-1/2} \tag{1}$$

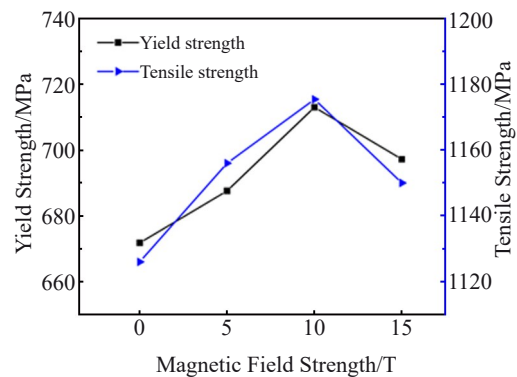


Fig.12 Effect of magnetic field strength on yield strength and tensile strength of GH99 alloys

where σ_y is the yield strength, σ_0 is the friction strength of the lattice, d is the grain size, and k is the Hall-Petch coefficient. The k value is related to the material, so it is a constant in this research. According to Eq.(1), the grain size of GH99 nickel-based alloy specimens is negatively related to the yield strength, and the grains are refined after the pulsed magnetic treatment. The tensile strength also increases after the pulsed magnetic treatment, and the yield strength reaches the highest value when the magnetic field strength is 10 T. The increment in tensile strength of the specimen with pulsed magnetic treatment at 10 T is 49.4 MPa, compared with that without pulsed magnetic treatment. This increment is attributed to the refinement of grain size to a certain extent which is caused by the pulsed magnetic treatment. Consequently, the material deformation occurs in more grains under the same condition, and the increase in grain boundaries is not conducive to the crack propagation.

2.3 Effect of pulsed magnetic treatment on hardness of GH99 alloy

Fig. 13 shows the statistical graphs of the Vickers hardness of GH99 alloys without and with pulsed magnetic treatment at different field strengths. The number of pulses is fixed as 20. The Vickers hardness HV of the specimen without pulsed magnetic treatment is 3977.428 MPa, and the hardness of GH99 alloys is firstly increased and then decreased with increasing the magnetic field strength. The maximum Vickers hardness is 4081.083 MPa when the magnetic field strength is 10 T. In practical engineering, the Vickers hardness is usually defined as the resistance to the penetration of hard ball. The deformation resistance of GH99 nickel-based alloy increases due to the changes in internal dislocations caused by the pulsed magnetic treatment. The pulsed magnetic treatment leads to the proliferation of dislocations, which are denoted as linear defect, in material, thereby increasing the deformation and directly increasing the material hardness. Additionally, the increase in dislocations also raises the possibility of interactions (cross-cutting and entanglement) between dislocations, which hinders the movement of other dislocations, resulting in a “process hardening-like” phenomenon. Moreover, the excessive dislocations at grain boundaries result in the

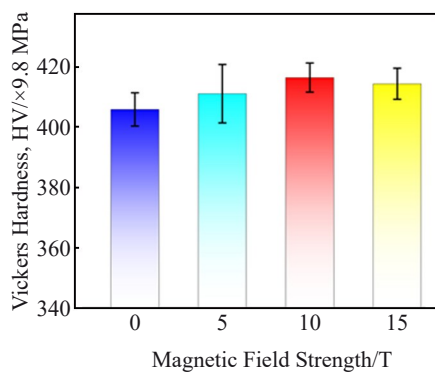


Fig.13 Vickers hardness of GH99 alloys without and with pulsed magnetic treatment at different field strengths

plugging of sub-structural dislocation wall and the increase in internal stress, thereby presenting the hardening effect. However, the over-strong pulsed magnetic treatment also has a debonding effect on dislocations, resulting in dislocation annihilation and dislocation dispersion within the two-dimensional dislocation network. Partial dislocation multiplication and hardening effect are offset by this negative effect, so the hardness of the specimen with pulsed magnetic treatment at 15 T slightly decreases, compared with that at 10 T.

2.4 Effect of pulsed magnetic treatment on wear resistance of GH99 alloy

Fig.14 shows the friction coefficient curves of GH99 alloys without and with pulsed magnetic treatment at different field strengths. It can be seen that the friction coefficient curves of different specimens exhibit basically the same variation trends, which can be generally divided into three stages: the fast rising stage at the beginning of micro-motion, the fluctuation stage at the middle stage, and the stable stage at the end^[14]. In the initial fast rising stage, because the direct contact area is small, the friction coefficient is low. The micro-motion occurs due to the high hardness of the extrusion and shear of grinding balls by the destruction of material removal. Micro-convex appears on the contact interface between specimen and grinding ball, thereby increasing the possibility of contact and friction. Thus, the two-body action is strengthened, and the friction coefficient quickly increases to the maximum value. Although small differences exist in the actual friction processes, the durations are all relatively short. The fluctuation only occurs within the initial dozen cycles.

In the middle fluctuation stage, the friction coefficient of all specimens show a certain extent of sawtooth fluctuations, because the reciprocal micro-friction process in the plastic deformation of the alloy surface and the elastic coordination increases. Continuous hardening results in the improved brittleness and the shear is more likely to cause local regional damage, leading to particle flaking and increasing the friction resistance. At the same time, the abrasive chips are continuously broken and oxidized during the circulation process, playing a micro-bearing role to reduce the friction coefficient. However, the friction coefficients of specimens

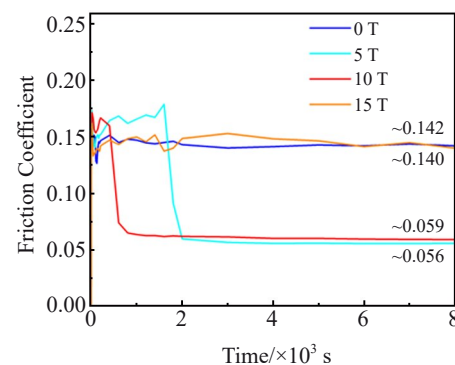


Fig.14 Friction coefficient curves of GH99 alloys without and with pulsed magnetic treatment at different field strengths

with pulsed magnetic treatment at 5 and 10 T suddenly decline, which is related to the change in the micro-running condition. In addition, the minimum friction coefficient can be achieved when the pulsed magnetic strength is 10 T, with less and shorter micro-cycles.

In the stabilization stage, a dynamic balance can be reached between the abrasive chips generated by friction. Abrasive chips are continuously compacted and accumulated into a protective third-body layer, which improves the wear resistance, reduces the shear stress on alloy surface, and gradually stabilizes the friction coefficient. As shown in Fig. 14, the friction coefficients of the specimens with pulsed magnetic treatment at 5 and 10 T are stabilized at 0.056 and 0.059 after 4×10^4 cycles, respectively, whereas those of the specimens without pulsed magnetic treatment and with pulsed magnetic treatment at 15 T are stabilized at 0.142 and 0.140, respectively. These results are related to the reduced grain size and increased Vickers hardness after pulsed magnetic treatment at 5 and 10 T. During the friction process, the specimens with pulsed magnetic treatment at 5 and 10 T have smaller abrasive grains, easily forming lubricant film with high hardness and high density on the surface of grinding balls and specimens. Therefore, the lower friction coefficient can be stably achieved, indicating the better wear resistance.

Fig. 15 shows the average friction coefficients and wear volumes of GH99 alloys without and with pulsed magnetic treatment at different field strengths. It can be seen that with increasing the magnetic field strength, the friction coefficient and wear volume are firstly decreased and then increased. The wear volume of the specimen without pulsed magnetic treatment reaches $1.71 \times 10^5 \mu\text{m}^3$ and its average friction coefficient is 0.144, indicating severe material loss, which are larger than those of the specimens with pulsed magnetic

treatment. The specimen with pulsed magnetic treatment at 5 T has wear volume of $6.06 \times 10^4 \mu\text{m}^3$, which is smaller than that without pulsed magnetic treatment by one order of magnitude. The ratio of wear volume of the specimen with pulsed magnetic treatment at 5 T to that without pulsed magnetic treatment is 0.36:1. The average friction coefficient of the specimen with pulsed magnetic treatment at 5 T reduces to 0.129. The specimen with pulsed magnetic treatment at 10 T has the average friction coefficient of 0.109, and its wear volume slightly reduces to $3.91 \times 10^4 \mu\text{m}^3$, indicating the mild wear. With further increasing the magnetic field strength to 15 T, the average friction coefficient is increased significantly, and the wear volume is also increased, which is even similar to that of the specimen without pulsed magnetic treatment. These results show that the wear volume of specimens after the pulsed magnetic treatment is reduced, indicating that the pulsed magnetic treatment can improve the wear resistance of the material. The wear volume of specimens with pulsed magnetic treatment tends to decrease, compared with that of the specimen without pulsed magnetic treatment, and the difference in wear volume of the specimens with pulsed magnetic treatment at 10 and 5 T is small. However, the wear volume of specimen with pulsed magnetic treatment at 15 T increases again, indicating that over-strong magnetic field strength is detrimental to the wear resistance of material. When the applied magnetic field strength exceeds a certain value, dislocation accumulation is too severe on the friction surface of specimen and thus the wear resistance deteriorates. Because the generation of crack sources directly accelerates the wear damage, the specimen with pulsed magnetic treatment at 15 T has larger wear volume than that at 10 T does. Therefore, the optimal magnetic field strength is 10 T.

To evaluate the wear degree of alloy specimens, the wear scar profile was also analyzed. The three-dimensional shapes of wear and the two-dimensional profiles along the center axis of the wear marks of the specimens without and with pulsed magnetic treatment at 5, 10, and 15 T are shown in Fig. 16. The areas above the substrate plane represent the chip accumulation projections. It is found that the chip accumulation of the specimens with pulsed magnetic treatment is mainly concentrated on the edges along the micro-motion direction, whereas the specimen without pulsed magnetic treatment shows a certain degree of chip accumulation around the wear marks. Fig. 16a shows that the profile curve of the non-pulsed magnetic treatment specimen presents the U-like shape, indicating the typical relative slip zone^[15], and the large center depth may be caused by the local stress concentration. The maximum depth of abrasion marks of the specimens without pulsed magnetic treatment is $6.04 \mu\text{m}$, and the large depression of the abrasion marks indicates the serious material loss. Fig. 16f–16h show the profile curves of the specimens with pulsed magnetic treatment at 5, 10, and 15 T, respectively. It is found that the abrasion depths of specimens with pulsed magnetic treatment at 5, 10, and 15 T are 4.183, 5.178, and $4.866 \mu\text{m}$, respectively, which are smaller than that of the specimen without pulsed magnetic treatment. After the

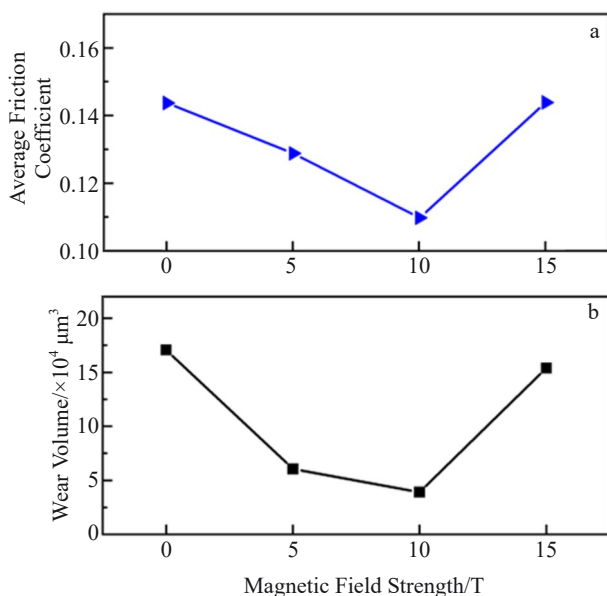


Fig. 15 Effect of magnetic field strength on average friction coefficient (a) and wear volume (b) of GH99 alloys without and with pulsed magnetic treatment at different field strengths

pulsed magnetic treatment, the dislocation proliferation leads to the increase in the dislocation density. Thus, the increase in the surface hardness also reduces the wear degree to a certain extent. It can also be seen that the contour curves of specimens after pulsed magnetic treatment all show the V shape, which is different from the U-like shape in Fig. 16e. This phenomenon is related to the final stabilization of their operation condition of partial slip. This result is consistent with the results of the friction hysteresis curves of different specimens in Fig. 17. The main characteristics of the contour profile of the specimens after the pulsed magnetic treatment are as follows: the depth of the central area of abrasion marks varies sharply with different amplitudes of fluctuation; the outer area of abrasion marks is relatively smooth, which is largely attributed to the hardening of some areas on the surface of specimens after pulsed magnetic treatment, resulting in different degrees of wear on the inner side of the crater during abrasion process. The contour shape of the specimens without pulsed magnetic treatment is more uniform, and the internal abrasion marks are flat.

In order to discuss the friction damage of different specimens, the wear volume is used to compare and analyze the differences in the wear rates. The wear rate is defined as the ratio of the wear volume of material to the friction work, and it can be calculated by Eq.(2)^[16], as follows:

$$K = \frac{V}{FDN} \quad (2)$$

where K is wear rate ($\mu\text{m}^3 \cdot \text{N}^{-1} \cdot \mu\text{m}^{-1}$), V is wear volume (μm^3), F is normal load (N), D is displacement amplitude (μm), and N is number of cycles. The wear rate can effectively characterize the size of wear. According to the test conditions in this research, the wear rates of the specimens without and with pulsed magnetic treatment at 5, 10, and 15 T are calculated as 3.55×10^{-3} , 1.26×10^{-3} , 0.81×10^{-3} , and $3.21 \times 10^{-3} \mu\text{m}^3 \cdot \text{N}^{-1} \cdot \mu\text{m}^{-1}$, respectively. It can be seen that the wear rate of the specimen with pulsed magnetic treatment at 10 T is 0.23

times higher than that of the specimen without pulsed magnetic treatment. This result further proves that the pulsed magnetic treatment can improve the wear resistance of material. The external pulsed magnetic field changes the internal stresses of the material, affects the plasticity, varies the rate of dislocation migration, and induces dislocation migration to the material surface, producing a process-hardening effect. Particularly, the most obvious process-hardening effect is achieved for the specimen with pulsed magnetic treatment at 10 T.

3 Discussion

3.1 Wear mechanism analysis

By changing the magnetic field strength, the friction hysteresis curves of different specimens are obtained. Fig. 17 shows the dynamic characteristics and basic information of micro-motion wear. As shown in Fig. 17a, the operation condition of the specimen without pulsed magnetic treatment mainly consists of relative slip form, and the friction hysteresis curve is approximately parallelogram. For the slip area, the surface is obviously worn under micro-motion friction condition. Fig. 17b and 17c show the friction hysteresis curves of specimens with pulsed magnetic treatment at 5 and 10 T, respectively. It can be seen that the relative slip form changes to the mixed slip form^[17], but those of the specimen with pulsed magnetic treatment at 10 T change to the mixed slip form earlier than that with pulsed magnetic treatment at 5 T. The mixed slip is characterized by a small relative slip between the friction surface of specimen and the counterpart, i.e., there is a slight slip at the edge of contact surface and no relative slip occurs between surfaces. This result also indicates that the wear degree is alleviated and the friction coefficient is decreased after the transformation from relative slip form to mixed slip form. Fig. 17d also shows the transformation from relative slip form to the mixed slip form, but the characteristics are not obvious. The frictional

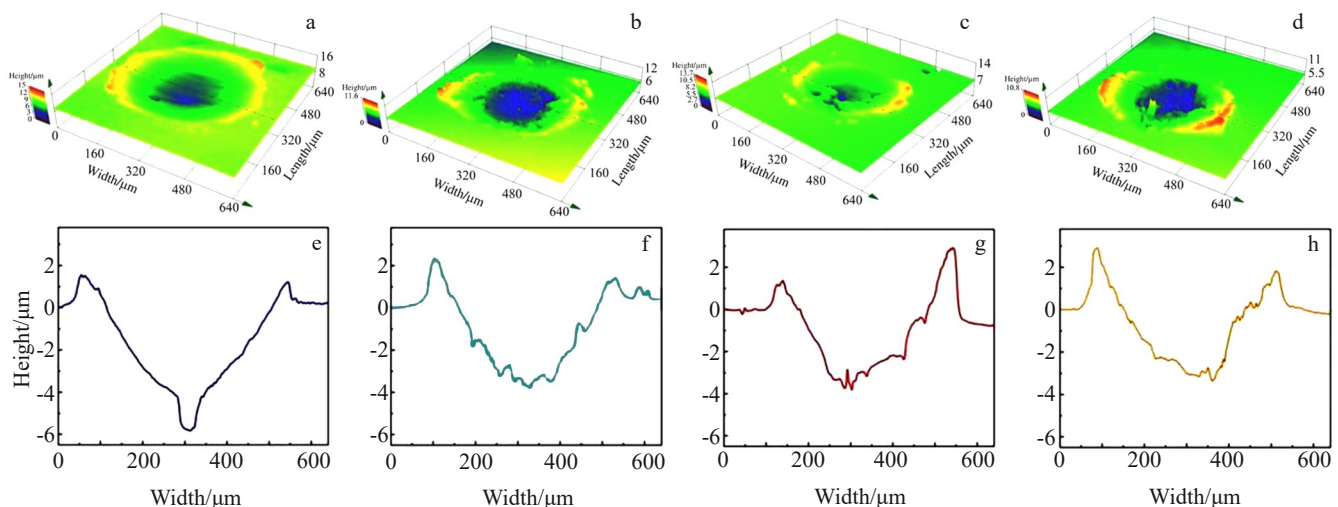


Fig. 16 3D morphologies (a–d) and 2D contour curves (e–h) of worn surfaces of GH99 alloy specimens without (a, e) and with pulsed magnetic treatment at 5 T (b, f), 10 T (c, g), and 15 T (d, h)

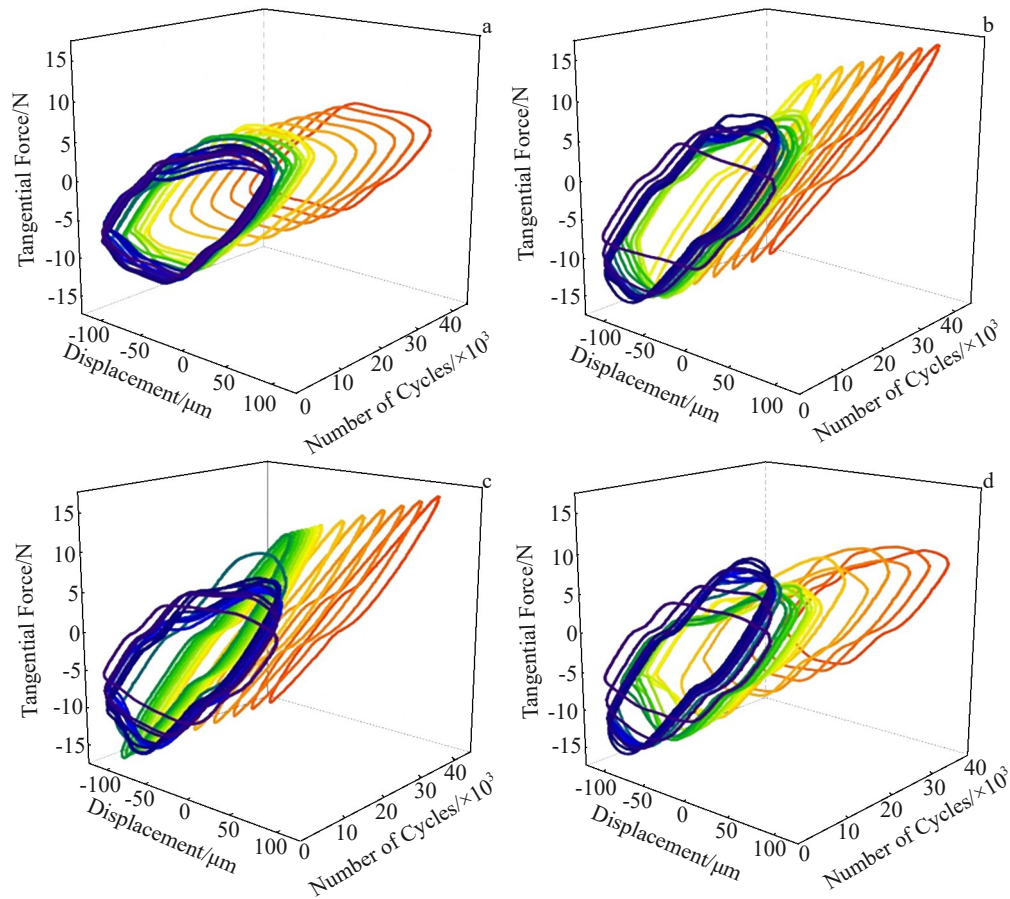


Fig.17 Frictional hysteresis curves of GH99 alloy specimens without (a) and with pulsed magnetic treatment at 5 T (b), 10 T (c), and 15 T (d) for 40 000 cycles

wear after pulsed magnetic treatment is reduced in the middle and stabilization stages, compared with that of the specimen without pulsed magnetic treatment.

The micro-motion wear mechanism of the specimens after pulsed magnetic treatment was further analyzed through SEM morphologies of wear marks, as shown in Fig.18. As shown in Fig. 18a₁–18d₁, the surface wear morphologies show a large area of white layer due to the severe process-hardening effect, which leads to the material embrittlement and brittle spalling. The white layer is further fragmented to form abrasive chips with smaller size in subsequent micro-action process, as shown in Fig. 18a₂–18d₂. At the same time, all specimen surfaces show plow grooves, which suggests that different specimens have different degrees of abrasive wear^[18]. The particle size of the specimen without pulsed magnetic treatment is larger than that of the specimens with pulsed magnetic treatment. Usually, when the particle size of the abrasive grain is less than 100 μm in the three-body wear: the smaller the particle size, the slower the surface wear rate. In addition, the grooved abrasion marks of the specimen without pulsed magnetic treatment are significantly larger in depth than those of other specimens, and the abrasive grain wear form has greater effect on the wear of the specimen without pulsed magnetic treatment. The resistance of furrow effect is the main component of surface friction. Fig.18a₃ shows the

plough grooves of specimen without pulsed magnetic treatment. A large area of spalling can be observed. In the process of abrasive wear, extruded flaking can be found in the local area of specimen with pulsed magnetic treatment at 5 T, and the flaking debris appear in the form of scales, as shown in Fig.18b₃, because the specimen plasticity is improved after pulsed magnetic treatment. Thus, the pulsed magnetic treatment can alleviate the damage to the specimen surface by abrasive wear to some extent.

In addition, there are abrasive spots adhering to a certain area, presenting the obvious adhesion effect, and adhesive wear occurs, in addition to abrasive wear. Fig.19 shows SEM wear surface morphology and the corresponding EDS element distributions of the specimen without pulsed magnetic treatment. It can be concluded that the abrasive spots mainly contain the oxygen and silicon elements, and Si₃N₄ ceramic balls adhere to the specimen surface during the micro-motion friction process, which reveals that the micro-friction damage mechanism of GH99 Ni-based alloy under non-lubricated conditions shows the multi-factorial damage behavior, mainly including abrasive wear, adhesive wear, and oxidation wear. These spots can fill the cracks, as shown in Fig.18c₃, which are similar to the action of solid lubricants and thus protect the wear surface. However, excessive thick spots can also form cracks during wear due to stress concentration, as shown in

Fig.18d₃.

3.2 Strengthening mechanism analysis of mechanical properties and wear resistance

The pulsed magnetic field can affect the dislocation of GH99 nickel-based alloy due to following reasons. Firstly, the pulsed magnetic field forms a swirling current on the surface of specimen, and the Lorentz force formed by the current and the magnetic field generates magnetic pressure to drive the dislocation motion. Secondly, the pulsed magnetic field

reduces the dislocation deformation force and thus increases the possibility of dislocation motion. By influencing the dislocation motion, the dislocation density of the material increases, and the dislocation morphology and distribution change to strengthen the mechanical properties and wear resistance of the material.

To investigate the effect of pulsed magnetism on the dislocation density of material, XRD patterns of the specimens without and with pulsed magnetic treatment at

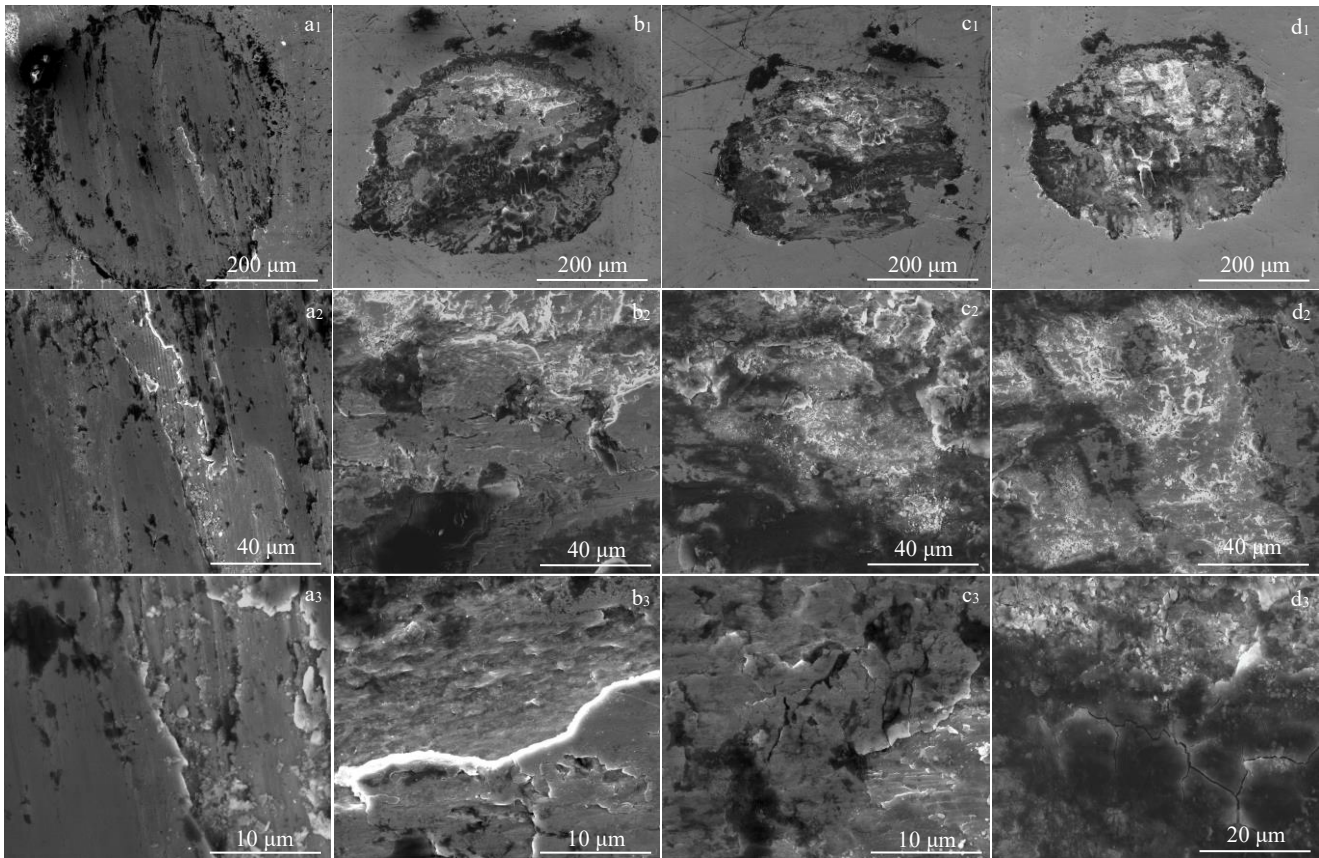


Fig.18 SEM wear morphologies of GH99 alloy specimens without (a₁-a₃) and with pulsed magnetic treatment at 5 T (b₁-b₃), 10 T (c₁-c₃), and 15 T (d₁-d₃)

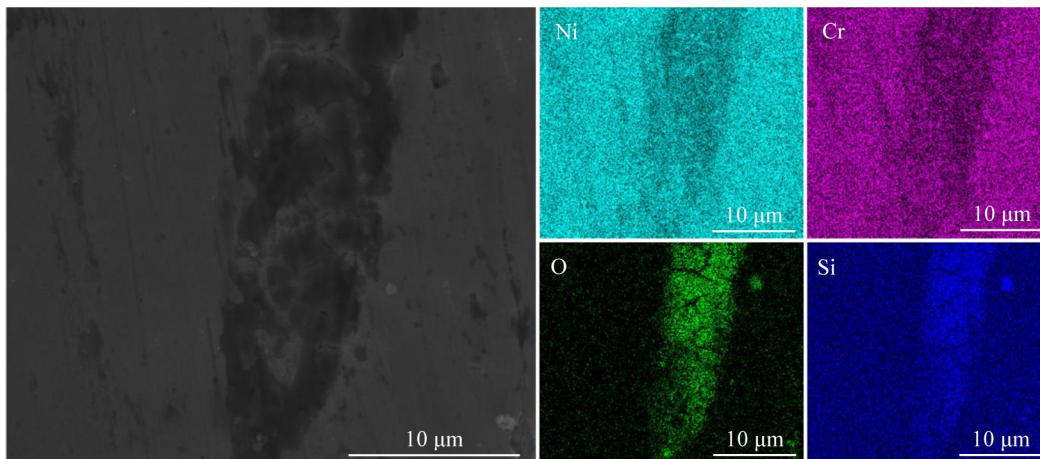


Fig.19 SEM wear morphology and EDS element distributions of GH99 alloy specimen without pulsed magnetic treatment

different field strengths were detected and analyzed, as shown in Fig.20. It can be seen that no new phases are generated after the pulsed magnetic treatment. However, the half-height width of the diffraction peaks of different specimens changes significantly. The half-height width of specimen with pulsed magnetic treatment at 10 T is the largest, whereas the narrowest half-height width is achieved for the specimen without the pulsed magnetic treatment. The specimens with pulsed magnetic treatment at 5 and 15 T show different degrees of broadening. The dislocation density D can be analyzed by the value of Burgers vector b and half-height width l , as expressed by Eq.(3):

$$D = \frac{l^2}{4.35b^2} \quad (3)$$

It can be concluded that based on the Frank-Read multiplication mechanism, the dislocation density of the material increases after the pulsed magnetic treatment, and dislocations are more likely to move when the specimens are subjected to the pulsed magnetic fields of different magnetic field strengths, due to the reduced opening resistance and the external drive force by electromagnetic force. During the process of dislocation proliferation, the morphology of dislocations also changes. Without pulsed magnetic treatment, most dislocation morphologies inside the specimen are dominated by the sparse and disordered linear dislocations, as shown in Fig.21a, and the dislocation density is the lowest. A small number of dislocation loops can be observed under the pulsed magnetic field at 5 T, as shown in Fig. 21b. The

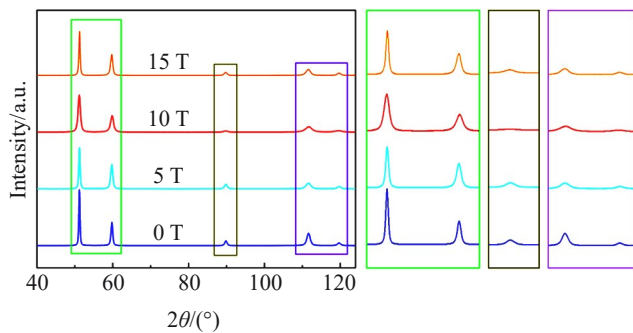


Fig.20 XRD patterns of GH99 alloy specimens without and with pulsed magnetic treatment at different magnetic field strengths

dislocation entanglements with less dense distribution can be found. When the specimen is processed by pulsed magnetic treatment at 10 T, a large number of dislocations appear, and numerous dislocations are entangled with each other when the slip opens subsequently. At the same time, the ring dislocations of high density can be observed, as well as a large number of dense dislocation areas and dislocation plugging group, as shown in Fig.21c. As shown in Fig.21d, the degree of dislocation entanglement in specimen with pulsed magnetic treatment at 15 T slightly reduces, compared with that at 10 T, and the over-strong field strength promotes the dislocation depinning effect, resulting in annihilation or dispersion of partial dislocations in the 2D dislocation network^[19]. The difference in dislocation morphologies is closely related to the dislocation properties. Usually, the dislocation plugging groups with high dislocation density and high degree of dislocation entanglement increase the deformation resistance under external forces, leading to the strengthening effect. In addition, with increasing the magnetic field strength, the dislocation density is raised by increasing the dislocation movement distance to generate new dislocation sources, which also contributes to the performance improvement of materials.

According to Fig. 22, a large number of spherical second phases exist in the matrix of GH99 nickel-based alloy, which are rich in Ni, Al, and Ti elements, inferring the age-hardened precipitation phase $Ni_3(Al, Ti)$, namely, the γ' phase of GH99 nickel-based alloy^[20]. Yang et al^[21] found that the critical size of γ' phase in GH99 nickel-based alloy cut by dislocation transition is about 60 nm. In Fig.22, the average grain size of γ' phase is about 70 nm, and it has high anti-phase domain energy and strong resistance against dislocation cutting. Under the experiment conditions in this research, the mechanism is that the enhanced phase cuts the dislocations, rather than the dislocations cut the γ' phase.

Fig. 23 shows TEM dark-field image of GH99 alloy specimens without and with pulsed magnetic treatments. A large number of reinforced phases exist in the matrix of the specimen without pulsed magnetic treatment, and the dislocations barely exist. As shown in Fig. 23b, a small number of dislocations in the specimen with pulsed magnetic treatment at 5 T are generated between the reinforced phases and they are cut into fine linear dislocations. Fig.23c shows the dislocation distribution of the specimen with pulsed

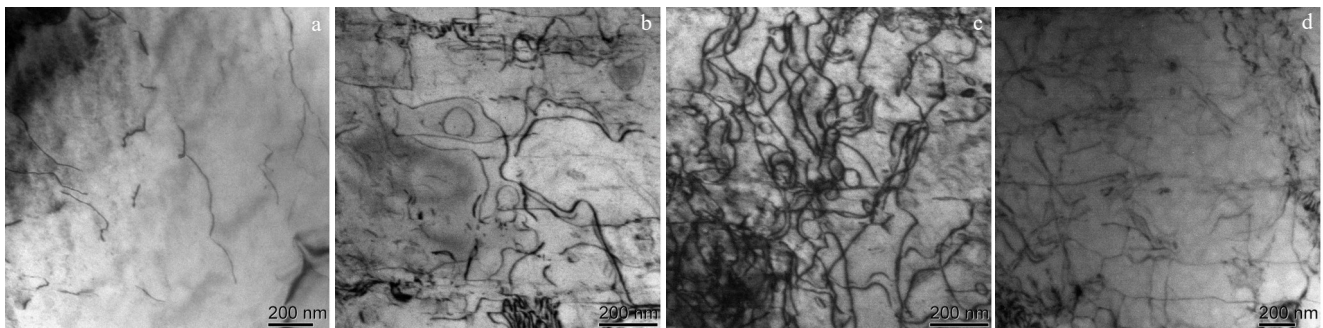


Fig.21 Dislocation morphologies of GH99 alloy specimens without (a) and with pulsed magnetic treatment at 5 T (b), 10 T (c), and 15 T (d)

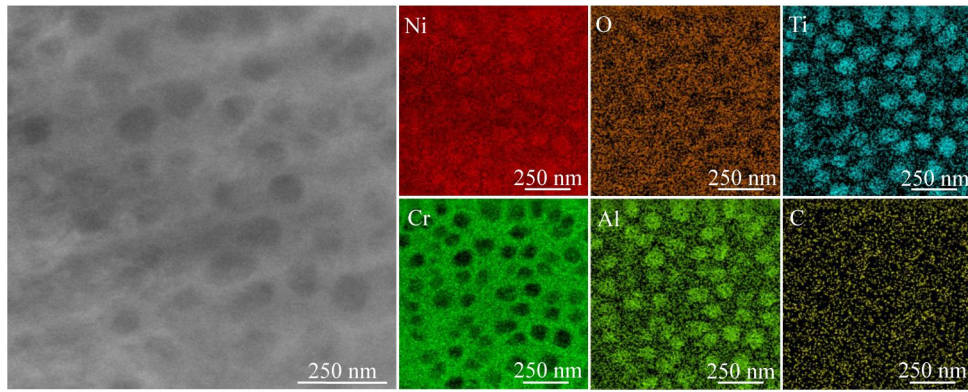


Fig.22 TEM morphology and EDS element distributions of enhanced phase

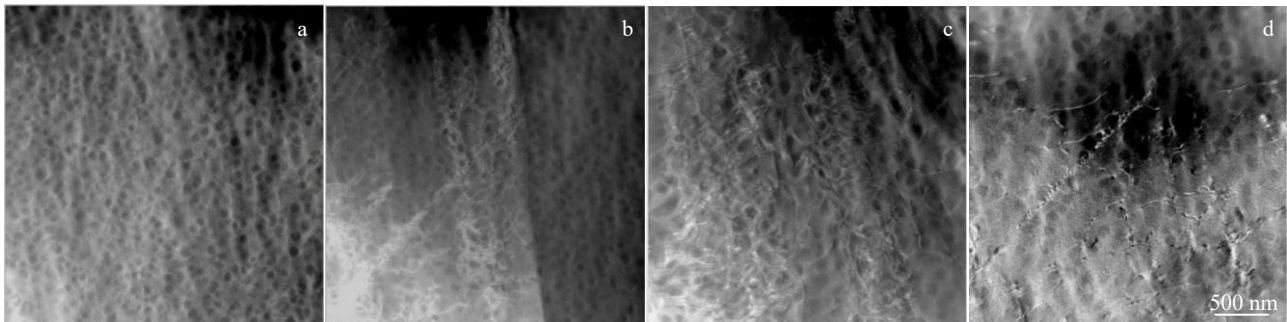


Fig.23 TEM dark-field dislocation distributions of GH99 alloy specimens without (a) and with pulsed magnetic treatment at 5 T (b), 10 T (c), and 15 T (d)

magnetic treatment at 10 T. A large number of dislocations are entangled, forming the dense dislocation area. According to Fig.23d, the dislocation density of the specimen with pulsed magnetic treatment at 15 T decreases, compared with that at 10 T, but a small amount of dislocation entanglement still exists. It is found that the strength contributed by the γ' phase in GH99 alloy accounts for about 20% of the total strength^[22]. The γ' phase has high strength characteristic. Moreover, the interfacial energy between γ' phases is relatively low, which causes good tissue stability under pulsed magnetic treatment. When the pulsed magnetic field causes dislocation movement, the γ' phase of the metal compound, which is highly dispersed in the matrix, can interact with the slipping dislocations due to its high hardness, thus forming obstacle to the dislocation slippage^[23]. This result is proved by the cutting effect of the reinforced phase particles on the dislocations. Dislocation rings are generated around the dislocation phase when the dislocations bypass the particles, and the dislocation density is increased by the Orowan mechanism, thus improving the properties of GH99 nickel-based alloy. When the magnetic field strength increases, the dislocations are more likely to move, which raises the probability of dislocations being cut by the particles in the reinforced phase, and thus the dislocations are proliferated. The dislocation ring acts as a new source of dislocations driven by the pulsed magnetic field and increases the dislocation density inside the specimen to some extent. The effect of the pulsed magnetic field treatment

on the effective distance l between the particles of reinforced phase should also be considered. The relationship between the curvature radius $l/2$ and the Orowan stress τ_0 is expressed by Eq.(4), as follows:

$$\tau_0 = \frac{Gb}{l} \quad (4)$$

where G is the shear modulus of substrate. The yield strength of the reinforced phase particles can be expressed by the Orowan stress τ_0 . According to Eq.(4), it is found that reducing the effective distance l between the reinforced phase particles indirectly increases the yield strength of reinforced phase particles. When the pulsed magnetic field is applied on the material through the magneto-vibration effect, the distance between the reinforced phase particles reduces to a certain extent, which increases the yield strength of the reinforced phase particles and dislocations, thus improving the cutting and blocking effect of the reinforced phase particles on dislocations. This result causes more dislocations to be cut, leading to the increase in the dislocation density of the specimen after the pulsed magnetic field treatment. In addition, under the pulsed magnetic field treatment, GH99 nickel-based alloys are subjected to different tensile and compressive stresses due to asynchronous expansion and mismatch deformation rates between the matrix γ phase and the reinforced phase, resulting in micro- and nano-scale vacancies between the matrix and the reinforced phase. As a result, a large number of dislocations accumulate around the

reinforced phase, and this phenomenon is also consistent with the dislocation distributions in Fig.23.

Fig.24 shows the characteristic organization of sparse and dense dislocation areas of specimen with pulsed magnetic treatment. It can be seen that the dislocation cell structure appears inside the specimen grains with pulsed magnetic treatment. The dislocation distribution inside the grains is not uniform, and there are high and low dislocation density regions. The low dislocation density region is the intermediate channel of the dislocation cell, and the high dislocation density region is the wall of the dislocation cell^[24]. When the abovementioned high dislocation density regions and low dislocation density regions alternately exist inside the grains, the dislocation cell structure of different sizes is generated inside the grain. This is because the dislocations slip and move under the pulsed magnetic action, and they may be

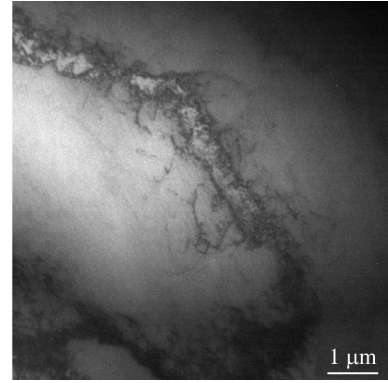


Fig.24 Characteristic organization of sparse and dense dislocation areas of GH99 alloy specimen with pulsed magnetic treatment

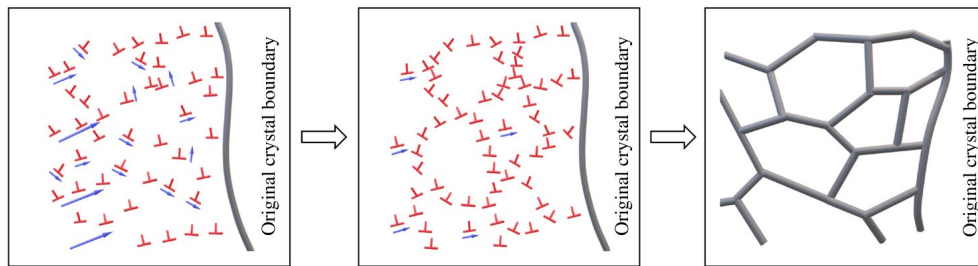


Fig.25 Schematic diagrams of continuous dynamic recrystallization

entangled with the non-motorized dislocations within the grains. When the subsequent driven dislocations meet the leading driven dislocations of the same number, they are arranged in a certain order around the entangled dislocations due to the mutual repulsion, forming the dislocation plugging phenomenon which is similar to that at the grain boundary. The dislocation plugging area is the dense dislocation area in Fig.24. By applying the pulsed magnetic field, the dislocations continuously move because the work done in the high dislocation density region is different from that in the low dislocation density region. The pulsed magnetic field causes the dislocations in the low dislocation density region to proliferate, resulting in the disappearance of dislocations in the high dislocation density and thereby the overall uniform distribution of dislocations within the material. The dislocations are gradually aligned and produce substructures inside the grain, such as cytosolic organization (dislocation cells) and subcrystalline organization^[25]. The subcrystalline boundary and cell wall structure lead to the change in the orientation difference after the continuous absorption of dislocations, and the further refinement of the grains occurs. This is the mechanism of continuous dynamic recrystallization nucleation, as shown in Fig. 25. The larger the number of dislocation cell substructures inside the grains, the more the dislocations to be balanced, and the more obvious the reduction in residual stress dispersion. The uniform distribution of residual stress has a significant effect

on the wear resistance of GH99 nickel-based alloy and reduces the possibility of premature crack formation due to the force concentration in the material. These results all show that the pulsed magnetic treatment can improve the wear resistance of GH99 nickel-based alloy to some extent.

4 Conclusions

1) With increasing the magnetic field strength from 5 T to 15 T, the range of the surface residual stress of GH99 nickel-based alloy is firstly increased and then decreased. At magnetic field strength of 10 T, the distribution range of the residual stress is the smallest, the stress distribution is the most uniform, the tensile fracture is mainly ductile fracture, the plasticity is optimal, and the post-fracture elongation and section shrinkage are 21.9% and 10.5%, respectively, which are higher than those of the specimen without magnetic field strength. However, the plasticity slightly decreases when the pulsed magnetic field strength is 15 T, compared with that at 10 T, indicating that the plasticity enhancement effect is not positively correlated with the magnetic field strength. The hardness is increased with increasing the magnetic field strength from 0 T to 10 T, indicating that there is a certain competitive mechanism between dislocation strengthening and dislocation de-pinning.

2) With increasing the magnetic field strength from 5 T to 15 T, the wear resistance is firstly increased and then decreased. At pulsed magnetic field strength of 10 T, the

surface wear volume of GH99 nickel-based alloy is the smallest. The mechanism is that the dislocation multiplication leads to the uniform surface stress distribution, reducing the stress concentration in local area and slowing down the wear process. The small increase in hardness also contributes to the wear resistance of the surface. In addition, the magnetoplastic effect enhances the material plasticity, thus preventing cracking and reducing the wear.

3) Pulsed magnetic treatment on GH99 nickel-based alloy increases the dislocation density and improves the dislocation distribution, thus enhancing the mechanical properties and wear resistance of GH99 alloy.

References

- Peng Zhenxun, Wang Zhanwei, Yan Jun et al. *Rare Metal Materials and Engineering*[J], 2022, 51(9): 3419 (in Chinese)
- Qin Shengxue, Zhao Ruirui, Zhang Hongbin et al. *Journal of Materials Heat Treatment*[J], 2017, 38(2): 55 (in Chinese)
- Qin Shengxue, Wang Yan, Zhang Hongbin et al. *Metal Heat Treatment*[J], 2020, 45(8): 173 (in Chinese)
- Zhao Wenxiang, Yao Hongmin, Liang Zhiqiang et al. *Journal of Beijing University of Technology*[J], 2014, 34(7): 661 (in Chinese)
- Wang Y, Xing Z G, Huang Y F et al. *Journal of Magnetism and Magnetic Materials*[J], 2021, 538: 168248
- Zhang Y F, Fang C Y, Huang Y F et al. *Journal of Magnetism and Magnetic Materials*[J], 2021, 540: 168327
- Sun Zhonghao, Xing Shuqing, He Shuai et al. *Rare Metal Materials and Engineering*[J], 2022, 51(1): 273 (in Chinese)
- Wang Xingmao, Ding Yutian, Gao Yubi et al. *Rare Metal Materials and Engineering*[J], 2022, 51(1): 249 (in Chinese)
- Wu Su, Zhao Haiyan, Lu Anli et al. *Journal of Tsinghua University, Natural Science Edition*[J], 2002, 40(2): 147 (in Chinese)
- Xu Qingdong, Li Kejian, Cai Zhipeng et al. *Journal of Metals*[J], 2019, 55(4): 489 (in Chinese)
- Sun Zhonghao, Xing Shuqing, Cheng Qiao et al. *Rare Metal Materials and Engineering*[J], 2022, 51(9): 3336 (in Chinese)
- Song Zhikun, Liu Yuanfu, Chen Deqiang et al. *Rare Metal Materials and Engineering*[J], 2022, 51(7): 2654 (in Chinese)
- Ding Yutian, Zhang Xia, Gao Yubi et al. *Rare Metal Materials and Engineering*[J], 2022, 51(10): 3732 (in Chinese)
- Lesnevskiy L N, Lyakhovetskiy M A, Savushkina S V. *Journal of Friction and Wear*[J], 2016, 37(3): 268
- Zhou Xianhui, Sun Yousong, Wang Wanshun. *Journal of Tribology*[J], 2016, 36(5): 650 (in Chinese)
- Xiong Dansheng, Li Xibin. *Powder Metallurgy Materials Science and Engineering*[J], 1996, 1(1): 49 (in Chinese)
- Liu Yanfei. *Study of SMA/Resin Interfacial Bonding Performance and Frictional Properties of Metal Interfaces*[D]. Harbin: Harbin Engineering University, 2018 (in Chinese)
- Zheng Chong, Liu Huimin, Lv Chunda et al. *Rare Metal Materials and Engineering*[J], 2022, 51(11): 4213 (in Chinese)
- Cai Z P, Lin J A, Zhou L A et al. *Materials Science and Technology*[J], 2004, 20(12): 1563
- Hu Liang, Wang Jue, Ju Jia et al. *Rare Metal Materials and Engineering*[J], 2022, 51(11): 4219 (in Chinese)
- Yang Sen, Wei Yuhuan, Song Chengyi et al. *Acta Metallurgica Sinica*[J], 1986, 22(6): 29 (in Chinese)
- Wang Huailiu. *Special Steel Technology*[J], 2006, 12(1): 30 (in Chinese)
- Yang Jinlong, Long Anping, Xiong Jiangying et al. *Rare Metal Materials and Engineering*[J], 2022, 51(3): 1031 (in Chinese)
- Li Guirong, Wang Fangfang, Zheng Rui et al. *Journal of Materials Research*[J], 2016, 30(10): 745 (in Chinese)
- Ma Yuanjun, Ding Yutian, Yan Kang et al. *Rare Metal Materials and Engineering*[J], 2022, 51(9): 3289 (in Chinese)

脉冲磁场强度对GH99镍基合金力学和微动磨损性能的影响

周安阳¹, 黄艳斐¹, 郭伟玲¹, 邢志国¹, 王海斗^{1,3}, 王志远⁴, 张艳芳²

(1. 陆军装甲兵学院 装备再制造技术国防科技重点实验室, 北京 100072)

(2. 中国人民解放军总医院 第七医学中心 口腔科, 北京 100000)

(3. 陆军装甲兵学院 机械产品再制造国家工程研究中心, 北京 100072)

(4. 哈尔滨工业大学 材料科学与工程学院, 黑龙江 哈尔滨 150001)

摘要: 为研究不同磁场强度对镍基合金力学性能和耐磨性能的影响规律, 在脉冲强磁场设备上对GH99镍基合金试样进行脉冲磁处理。通过观察显微结构, 分析了GH99镍基合金的磨损机理和强化机制。结果表明: 外加脉冲磁场可改善材料位错分布, 减小试样表面残余应力的分散性; 在磁场强度为10 T时残余压应力达到最大值(-223.45 MPa), 且此时材料拉伸断口的特征主要表现为韧性断裂, 脉冲磁场处理合金产生亚结构位错胞有助于发挥细晶强化作用; 在0~15 T范围内, 随磁场强度增大, 材料表面显微硬度和耐磨性能呈现先增强后减弱的规律, 在脉冲磁场作用下合金材料内部的位错发生增殖致使位错密度增大, 产生类似加工硬化现象, 但磁场强度过大会导致位错塞积而造成晶胞点阵畸变严重, 出现材料性能恶化。

关键词: 脉冲磁场; 磁场强度; GH99镍基合金; 力学性能; 耐磨性能

作者简介: 周安阳, 男, 1993年生, 硕士, 陆军装甲兵学院装备再制造技术国防科技重点实验室, 北京 100072, E-mail: a603153081@qq.com